"This document is the unedited Author's version of a Submitted Work that was subsequently accepted for publication in Molecular Pharmaceutics, copyright © American Chemical Society after peer review. To access the final edited and published work see https://pubs.acs.org/doi/abs/10.1021/acs.molpharmaceut.8b01172."

Nano-confinement Effects on the Glass Transition and Crystallization Behaviors of Nifedipine

Sixue Cheng, Gregory B. McKenna*

Department of Chemical Engineering, Whitacre College of Engineering, Texas Tech University,

Lubbock, TX 79409-3121, USA

*Corresponding author

Department of Chemical Engineering, Whitacre College of Engineering, Texas Tech University,

Lubbock, TX 79409-3121, USA

Phone: 806.834.4136

Email: greg.mckenna@ttu.edu

Table of Contents Graphic

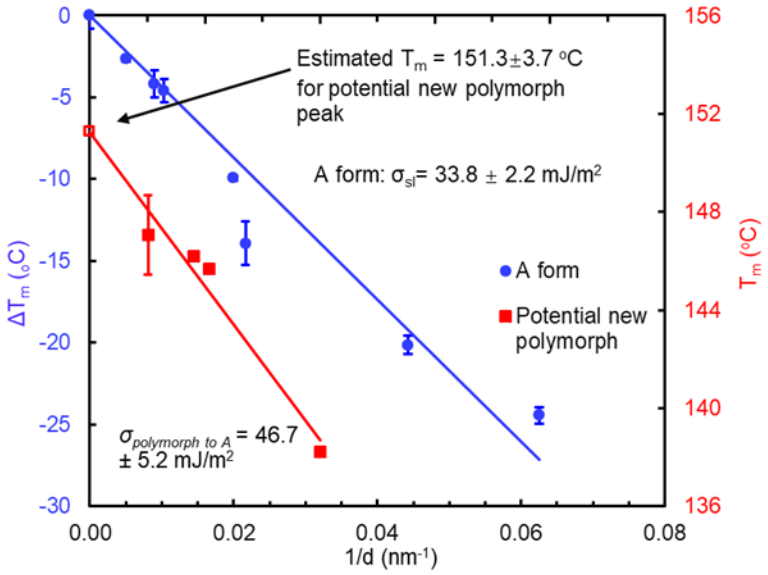

Abstract:

The impact of nanoconfinement on the crystallization and glass transition behaviors of nifedipine (NIF) has been investigated using differential scanning calorimetry. Nanoconfinement was provided by imbibing the NIF into a porous medium (controlled pore glass, CPG) and results were compared with the unconfined bulk material. Consistent with previous results from the literature, both glass transition temperature T_g and melting temperature T_m decrease with decreasing pore size. The melting temperature was found to decrease with the reciprocal of pore diameter and could be analyzed with the Gibbs-Thomson equation. In addition, for confinement sizes of 7.5nm and 12nm, it was found that no cold crystallization occurs upon heating from the glassy state to above the expected melting transition. Finally, at intermediate confinements we find evidence of a possible new, confinement-induced polymorph of NIF.

Keywords: Glass transition; Cold crystallization; Amorphous pharmaceutical; Polymorphism; Nifedipine

1. Introduction

The amorphous pharmaceutical is generally considered to have a higher water solubility and better bioavailability than the crystalline counterpart. As a result, the study of amorphous pharmaceuticals has become a subject of great interest, especially for those with poor solubilities in the crystalline state. However, amorphous pharmaceuticals tend to crystallize from the amorphous (glassy) state back to a lower energy crystalline state even at ambient temperatures. Therefore, to extend the shelf-life for processing and storage, a challenge faced by industry is to predict and prevent the amorphous pharmaceutical from reverting to the crystalline state. Re-crystallization from the glassy state or supercooled liquid, which occurs upon heating up to the normal melting temperature, is referred to as cold-crystallization. For a given heating rate, the cold-crystallization depends on the number of nuclei existing in the amorphous material [1-4], and reducing or avoiding nucleation would be expected to stabilize the amorphous pharmaceutical.

Hence, it is of interest to study how to enhance the solid-stability and suppress crystallization of amorphous pharmaceuticals [5-11]. Among the ways to do this, one method is to add a polymer additive to the amorphous pharmaceutical and make the system into an amorphous solid dispersion (ASD) mixture. Though, the mechanism of how the added macromolecule functions as a crystallization inhibitor is still poorly understood, it seems that one contribution is that the glass transition temperature T_g increases upon addition of the polymer, which reduces the molecular mobility and results in a more stable amorphous system [12-16]. At the same time, both crystallization and glass transition have been shown to be strongly affected by nanoscale confinement, and this offers another potential route to control the stability of the amorphous phase pharmaceutical.

For over 25 years, there has developed a significant body of work on the impact of nanoconfinement on the glass transition [17-26] and crystallization [27-30]. Relative to the bulk state, the materials confined at the nanoscale usually have a different glass transition temperature, both for polymeric and small molecule systems. For small molecule systems, it is commonly reported that T_g is

depressed by confinement in the nanoporous structure[17, 21, 26, 31]. For certain cases, even multiple glass transition temperatures are observed in the nanoconfined material[24, 32], and these have been attributed to the interaction between the confining medium and the studied material for the higher glass transition[30]. The lower one is thought to be due to an intrinsic size effect [31]. As regards crystallization, previous research shows that the kinetics and thermodynamics of crystallization at the nanoscale can have complicated crystallization modes, leading to the formation and stabilization of metastable polymorphs [29, 33-38]. Moreover, it has also been reported that nucleation inhibition can occur in the nanoconfined organic glass forming liquid [27, 28, 39]. Jackson and McKenna reported suppression of crystallization in benzyl alcohol confined in 4 nm controlled pore glass (CPG) and *o*-terphenyl confined in 8.5 nm CPG [40]. Similarly, nucleation suppression has been observed in acetaminophen confined to 4.6 nm pores[39].

In the present work, we use nifedipine (NIF) as a model to study the glass transition and cold-crystallization both in bulk and under nanoconfinement. NIF is a common calcium channel blocker and has been widely used in the pharmaceutical community to study crystallization from the amorphous state[41-46]. Previous studies show that, more than one crystal growth mode appears in the cold crystallization of NIF [45-49] and an abruptly fast crystal growth occurs at temperatures even below T_g. Such behavior makes NIF a complex but interesting model to study the glass transition and crystallization at the nanoscale. Here we report results from an investigation of the crystallization and glass transition behavior of the pharmaceutical nifedipine under nanoconfinement with the aim of increasing our understanding of stabilization in amorphous pharmaceuticals. The nanoconfinement in this work was achieved by filling NIF into different size CPGs, and the glass transition and cold crystallization were studied by differential scanning calorimetry (DSC). The results show that, NIF under nanoconfinement exhibits significant differences from bulk scale behaviors, in both glass transition and cold crystallization behaviors. Both glass transition temperature T_g and melting temperature T_m decrease with decreasing pore size, and two T_gs are also observed except for the smallest 7.5nm confinement. For the CPG pore sizes of

7.5nm and 12nm, no cold crystallization occurs upon heating from the glassy state to above the expected melting transition. For intermediate confinements evidence of a possible new, confinement-induced NIF polymorph is observed in the DSC thermograms.

2. Experimental Section

2.1 Materials and preparation methods

The Nifedipine used in this study came from Laborate Pharmaceutical Ltd, India. Both powder X-ray diffraction and DSC results (melting point = 172°C) indicated that as received, it is the pure A (α or I) form of NIF. The material was used as received without further purification. Controlled pore glasses (CPG) of nine different sizes 7.5, 12, 16.5, 22.6, 46.6, 50, 96.6, 111 and 198 nm, were used in the study. 7.5, 12, 16 and 50nm CPGs were supplied by Sigma-Aldrich, while the other sizes are from CPG, Inc. Before any usage, the CPGs were cleaned thoroughly by being immersed in 70% nitric acid at 110°C for 10 hours, washed with distilled, deionized water and then dried in a vacuum oven at 100°C for 24 hours [50].

Table 1 CPG manufacturer specifications and pore fullness calculations

pore size nm	±%	pore volume cm^3/g	Mesh size	100% fullness mass ratio NIF: CPG	60% fullness mass ratio NIF: CPG
7.5	13.5	0.49	200/400	0.63:1	0.38:1
12	10	0.68	80/120	0.88:1	0.53:1
16	12.1	1.13	20/80	1.47:1	0.88:1
22.6	6.2	0.85	120/199	1.10:1	0.66:1
46.6	6.4	0.98	120/200	1.27:1	0.76:1
50	10	1.1	80/120	1.40:1	0.84:1
96.6	6.8	1.02	120/200	1.31:1	0.79:1
111	6.9	1.02	120/199	1.32:1	0.79:1
198	7.2	0.91	120/200	1.18:1	0.71:1

Amorphous nifedipine was prepared by a melting and quenching procedure: the crystalline NIF was melted in a vacuum oven at 182 °C (about 10 °C above the melting point) and then quenched onto a precooled aluminum block at -10 °C (about 40 °C below the bulk NIF T_g). For the CPG nanoconfinement,

NIF liquid was imbibed into the CPGs via capillarity as follows: the CPGs were first placed in a small aluminum weighing dish (1.25-inch diameter, with a cover), and covered with the desired amount of NIF powder. Then the mixed NIF/CPG samples were heated in a vacuum oven at 185-190 ^{o}C for 10 mins, allowing the liquid NIF to flow into the pores. Both the masses of NIF powder and CPG were measured with a Scientech SA210 micro-balance having a precision of 0.1 mg. Similar to previous works [51], the actual fullness ratio of sample/CPG was generally lower than the theoretical value calculated from the pore volume provided by the CPG manufacturer. However, the pore fullness does not affect the change of T_g or T_m because the filling material forms plugs rather than layering caused by wetting of the pore walls [40, 50]. Considering this fact, to prevent overfilling, the mass ratio of NIF and CPG was used to calculate a value that allows the NIF to reach 60%-80% volume fullness of pores. For the 50nm diameter sample, the overfilling condition was also prepared to compare results with those obtained in the under-filling condition. The CPG specification from the manufacturers and fullness calculations are shown in Table 1. After preparation, all samples were placed in a jar containing Drierite as desiccant.

2.2 Thermal Analysis

To establish the thermal stability of the NIF, thermogravimetric analysis (TGA) was carried out for the bulk and 12nm confined NIF using a Mettler Toledo TGA2. To estimate the degradation temperature, both bulk and 12 nm confined NIF were heated from 110 ^{o}C to 350 ^{o}C at a 10K/min heating rate in a nitrogen atmosphere. Before the temperature scans, both samples were held in nitrogen at 110^{o}C for 20 min to exclude any moisture weight loss effects in the subsequent temperature scans. All subsequent preparation and testing were performed below the degradation temperature measured by TGA.

Calorimetric analysis was carried out using a Mettler Toledo DSC823e with nitrogen purge gas and Freon intra cooling system. Indium was used to calibrate the instrument before measurement, using a heating rate of 10K/min. And all heating scans were performed at 10K/min. Cooling rates of 3, 10, 20, 30 K/min were investigated. In the DSC measurements, the effective NIF amount ranged from 2.5mg to 7mg, Perkin Elmer Hermetic pans were employed to prevent any possible leaking. For all samples

measurements were performed at least 2 times on different samples from the same batch, and at least three DSC scans (N=6 in total) were carried out to insure repeatability and estimate a standard deviation.

2.3 X-ray Diffraction

Powder X-ray diffraction (PXRD) was also employed to characterize the as-received powder sample, a bulk glassy sample (prepared by melting and quenching, and made into powder using a pestle and mortar) and a 12nm confined sample at room temperature. The diffraction data were collected on a Rigaku Ultima III powder diffractometer. X-ray diffraction patterns were obtained by scanning a 2θ range of 5 -40°, step size = 0.02°, and scan time of 2.0 min/degree. The X-ray source was Cu Kα radiation (λ =1.5418 Å) with an anode voltage of 40 kV and a current of 44 mA. The beam was then discriminated by Rigaku's Cross Beam parallel beam optics to create a monochromatic parallel beam. Diffraction intensities were recorded on a scintillation detector after being filtered through a Ge monochromator. The samples were prepared as standard powder mounts and the diffractograms were processed through the software JADE v9.1. All PXRD measurements were performed at room temperature.

2.4 Data analysis

2.4.1 Glass transition temperature and Moynihan method

In this work, the glass transition temperature T_g was determined from the fictive temperature T_f, i.e., $T_g = T_f$. The value of fictive temperature was determined by applying the Moynihan area matching method to each heating curve[25, 52, 53]:

$$\int_{T_f}^{T \gg T_g} (C_{p.l} - C_{p,g}) dT = \int_{T \ll T_g}^{T \gg T_g} (C_p - C_{p,g}) dT \qquad (1)$$

Where $C_{p,g}$ and $C_{p,l}$ represent the glassy state heat capacity and liquid state heat capacity, respectively. C_p is the apparent heat capacity measured from experiment, T is temperature, T_f is fictive temperature and T_g is glass transition temperature. Through integration of both sides of equation (1) and comparison of the

integrated areas, the T_f point is determined when the right hand side is equal to the left hand side. Generally, slower cooling rate will cause a larger enthalpy overshoot during heating, leading to differences between fictive temperature from the Moynihan method and the glass transition temperature obtained from the midpoint method (half-height) [54].

2.4.2 Melting point depression and Gibbs-Thomson equation

The Gibbs[55] - Thomson[56] equation is a very common method to describe the melting point depression as crystal size decreases [57]. The expression for the change of melting point ΔT_m with crystal size is [50, 58]:

$$\Delta T_m = T_m - T_m(d) = \frac{A\sigma_{sl}T_m}{d\Delta H_f \rho_c} \qquad (8)$$

Here T_m is melting point of the bulk material, $T_m(d)$ is the melting point in the pore of diameter d, σ_{sl} is the solid- liquid interfacial energy, A is a geometry factor, which is 4 in the case of the CPG cylindrical pores [50, 59]; d is the pore diameter, ΔH_f refers to the bulk heat of fusion, which was obtained in the present study as 104.24±1.70 J/g, ρ_c is the density of the bulk crystal, where ρ_c = 1.29 g/cm^3 for nifedipine[18].

3. Results and Discussion

3.1 Thermogravimetric Analysis and PXRD

The PXRD results for the as-received sample and quenched sample are shown in Figure 1, together with other samples isothermally crystallized (Curve C to E), and which will be discussed in the section on crystallization. The diffraction pattern for the as-received NIF (Curve A in Figure 1) agrees with the A form NIF reported in the literature [60-62], indicating that the as-received sample is pure A form crystalline NIF. The bulk (Curve B) and 12nm confined NIF (Curve D) after melting and quenching

show a typical amorphous pattern, indicating that both for bulk and nanoconfined NIF, the material formed by quenching is amorphous NIF.

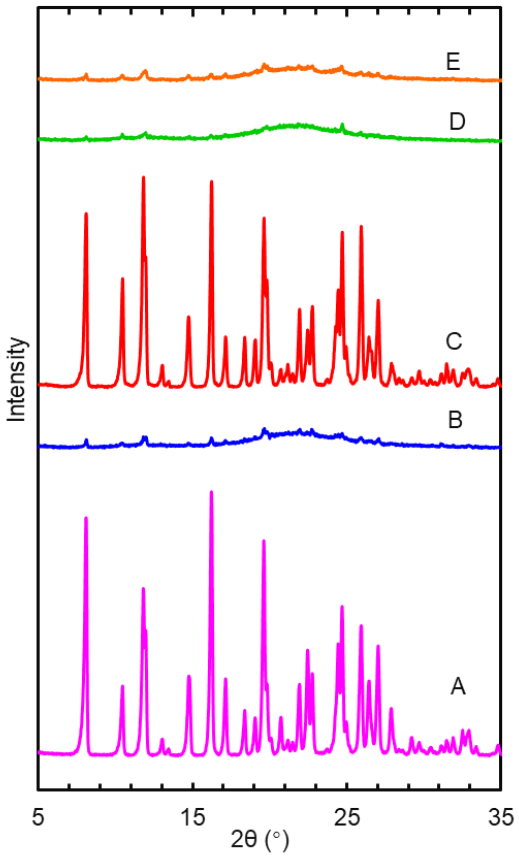

Figure 1. Powder X-ray diffraction patterns for (A) Pure bulk crystalline nifedipine as received from the manufacturer; (B) Bulk amorphous nifedipine after melting and quenching; (C) Bulk amorphous nifedipine, same as B after being held at 100 ºC for 2 hours; (D) Nifedipine confined in 12 nm nanopores after melting and quenching; (E) Nifedipine in 12 nm nanopore, same as D, after being held at 100 ºC for 2 hours.

In Figure 2, we present the TGA curves showing the thermal degradation of the bulk NIF and the 12nm pore confined NIF. All the TGA experiments were done in a nitrogen atmosphere. A 20-minute isothermal hold at 110 ºC preceded each heating ramp. The mass loss attributed to moisture in this step is less than 2%. The following heating scan was performed from 110 ºC to 350 ºC at 10K/min heating rate, which is the same heating rate used in the DSC experiments. The onset degradation temperature for the NIF was 256 ºC. The same procedure was also applied to the 12nm pore confined NIF, and the

degradation temperature was 266 ºC. From Figure 2 it can be seen that above the degradation temperature, the nanoconfined NIF has a slower weight loss rate, indicating that the nanoconfined NIF has a higher thermal stability. While it has been known that nanoconfinement can accelerate polymerization[63-65], it has been also widely reported that the thermal stability and flame-retardation of polymers is enhanced in nanocomposites systems [66-69], with enhancement being attributed to the hinderance of diffusion by nanoconfinement [67]. A study of poly(ethylene oxide) confined in anodic aluminum oxide (AAO) also showed a higher thermal degradation temperature[70], which is similar to the observation in the present work.

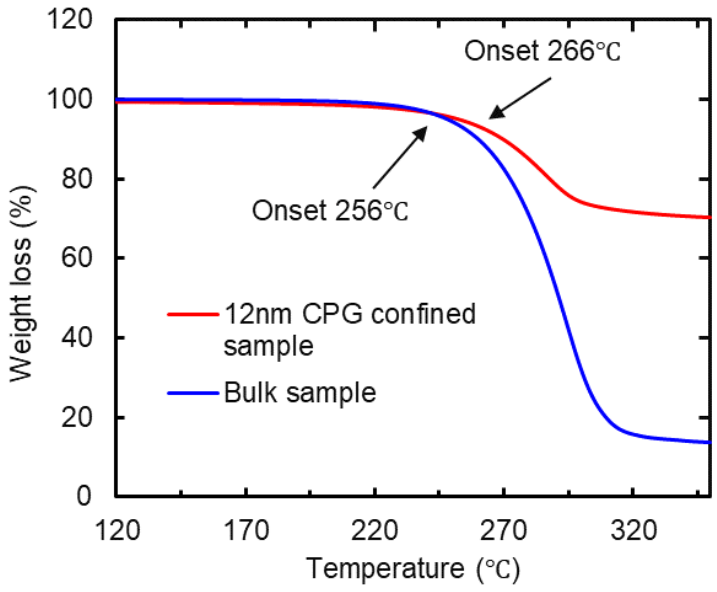

Figure 2. TGA curves for heating scans from 120 to 350 ºC at a heating rate of 10K/min for bulk and 12 nm CPG confined samples. Before measurement samples were held a 120 ºC for 20min to remove moisture and its effects on the heating scan weight loss measurements. The moisture weight loss was less than 2%.

We also performed an isothermal experiment at 200 ºC for both bulk and 12nm pore confined NIF. After one hour, no significant mass loss was observed in either case. Based on the degradation measurements, all experimental temperatures in the present study were kept below 200ºC to make sure that no thermal degradation occured during sample preparation and the DSC measurements.

3.2 Differential Scanning Calorimetry (DSC)

3.2.1 Glass Transition T_g and Confinement Effect on T_g

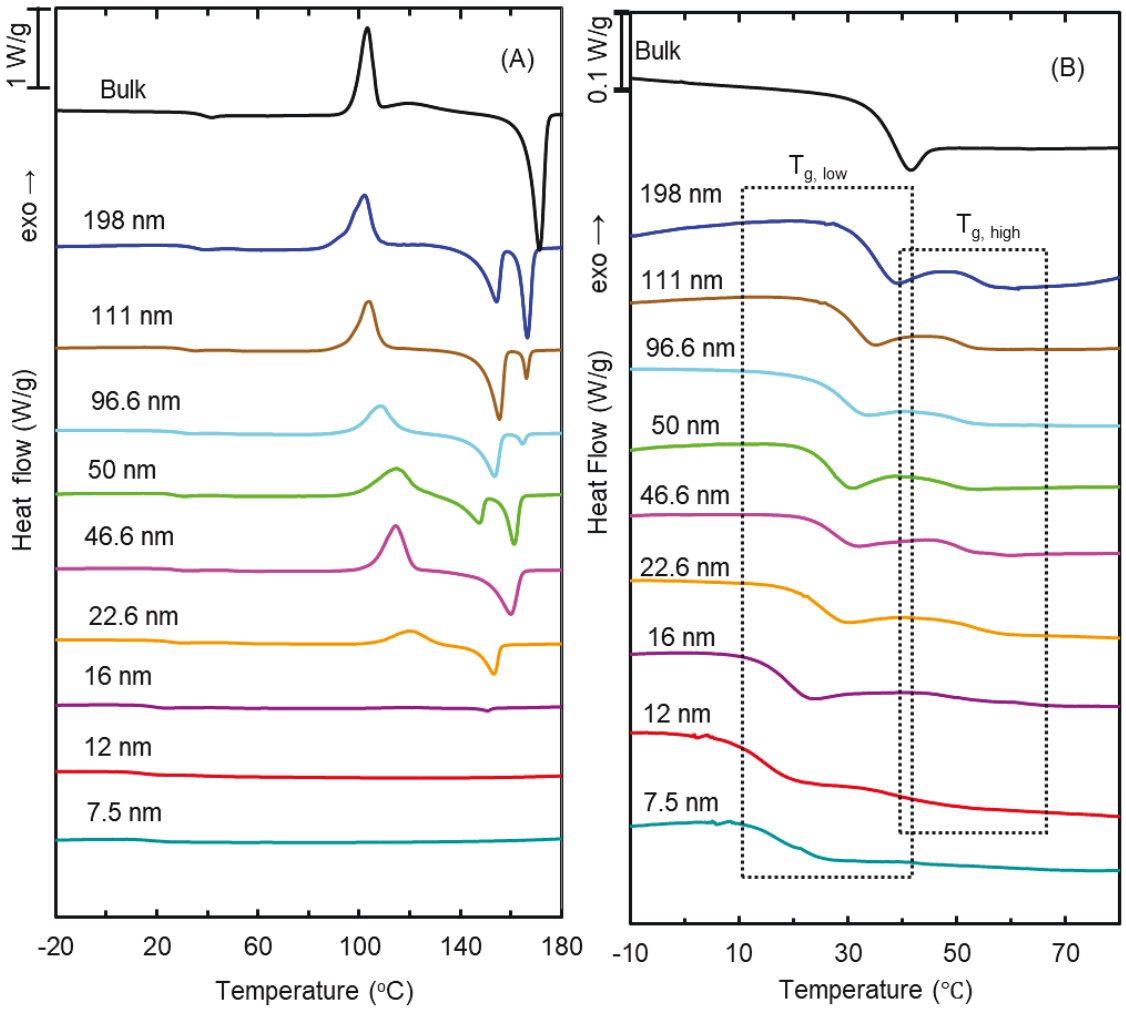

Figure 3 Full heating curves (A) of all, sample, both heating rate and cooling rate is 10K/min. Amplified glass transition region curve (B), all samples were heated at 10K/min heating rate after 10K/min cooling

While all heating was performed at 10K/min, different cooling rates were used in the thermal analysis. Among the results, a glass transition appeared on re-heating after quenching at cooling rates of 10, 20 and 30 K/min. When the cooling rate was reduced to 3K/min, no glass transition or cold crystallization were observed upon heating, rather melting peaks were seen, indicating that for the 3K/min

cooling rate, crystallization occurs during cooling and no glass is formed. To avoid this and insure that the NIF samples remained amorphous during cooling, subsequent measurements were performed with cooling rates of 10K/min or above. Typical DSC results for the heating curves for the NIF samples are shown in Figure 3(A), Figure 3(B) shows an amplification of the data of Figure 3(A) in the glass transition region. In Figure 3(B), it is apparent that for confinement sizes from 12 to 198 nm, two glass transitions are observed. The lower T_g ($T_{g,low}$) in the nanopore confined NIF falls in the temperature range from 17 to 31.3 ^oC, and is dependent of the confinement size. The confined $T_{g,low}$ was found to be lower than the bulk T_g of 38.3 ^oC. A second, higher T_g ($T_{g,high}$) emerges at a temperature of approximately 50±3 ^oC, which is higher than the bulk T_g, and is relatively independent of the pore diameter.

For the bulk sample, for a 10K/min cooling rate, the T_g was 38.3 ^oC, and for 30K/min cooling, the T_g was 41.0^oC, which is consistent with the literature[44, 45]. In the present work, we use the T_g value obtained from the 10K/min cooling rate. For the NIF confined in 198nm pores, the $T_{g,low}$ is 31.8^oC, i.e., compared with the bulk T_g, a reduction of 6.5K is observed. The $T_{g,low}$ for the 12nm confined NIF is lower than the bulk T_g by approximately 24.7K. The relationship of $T_{g,low}$ versus 1/d is shown in Figure 4(A). The observation of a decreasing $T_{g,low}$ with pore size is similar to the T_g reduction for o-terphenyl(*o*TP) and benzyl alcohol [17] in CPGs, where the $T_{g,low}$ of *o*TP was reduced by as much as18.2K compared to the bulk T_g. In addition, a 30K T_g reduction has been reported for cyanate ester confined in 8.1nm CPG and 50K for a polycynurate confined in the same size CPG [71]. While a significant confinement size dependence is observed for $T_{g,low}$, the confinement size does not have a comparable effect on $T_{g,high}$. As shown in Figure 4(C), $T_{g,high}$ for different confinement sizes varies over a narrow temperature range from 48 to 52 ^oC.

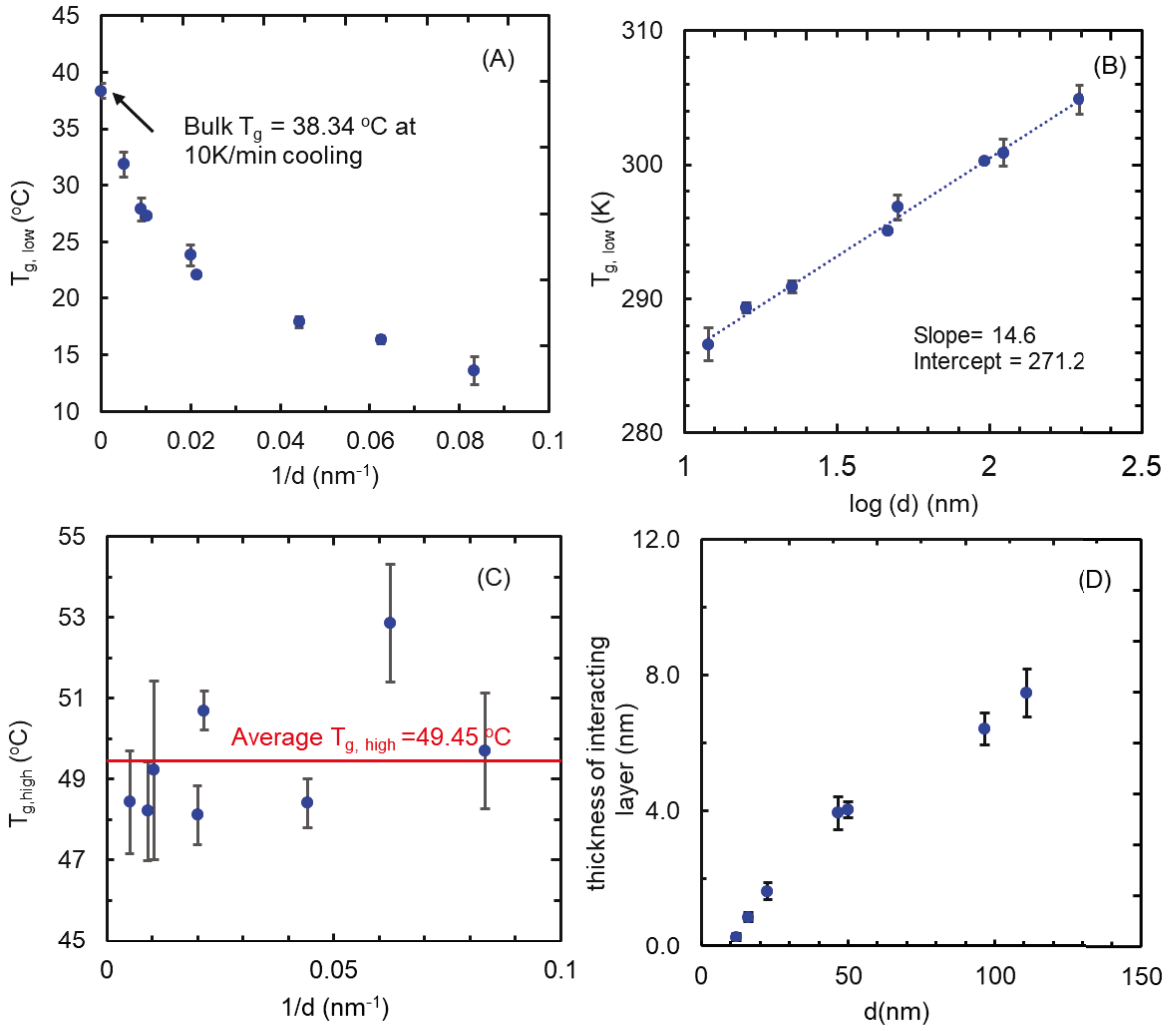

Figure 4. Glass transition temperatures $T_{g, low}$ and $T_{g, high}$ (A) lower glass transition temperature $T_{g, low}$ change as reciprocal of the pore diameter 1/d. (B). a linear relationship exhibit between $T_{g, low}$ and log (d). (C) the second glass transition temperature $T_{g, high}$ versus reciprocal pore diameter 1/d. (D) thickness of interacting layer (nm) versus reciprocal pore diameter d.

The above mentioned two T_gs have been commonly found in glass forming materials confined in porous media, including both polymers [18, 19, 21, 32] and small molecules [19, 23, 72]. To describe the phenomenon of two T_g s in porous nanoconfinement, a two-layer-model [30] was proposed. In the model, a core of confined material in the center of the pores is covered by an interfacial shell, which is a thin layer of material in contact with the wall of the CPG. The material in the core has a different molecular mobility from that in the shell and responds differently to temperature changes. The change of glass

transition is affected by the interaction between the confining walls and the material, as well as by the size of the confinement. In this case, for NIF in the core, a primary glass transition with $T_{g,low}$ occurs because of an intrinsic size effect [31]. At the same time, the NIF at the pore wall has a positive interaction with the wall, leading to a lower molecular mobility and a second glass transition with $T_{g,high}$ [22]. The sum of the heat capacity change $\Delta C_{p,\,total}$ of first and second glass transitions is close to the heat capacity change of the glass transition in bulk NIF obtained from the current study, which is 0.37J/g. The heat capacity change of the first glass transition $\Delta C_{p,\,low}$ is about two times higher than the heat capacity change of the second glass transition $\Delta C_{p,\,high}$. The fraction of material in the core and shell can be estimated from the ratio of the heat capacity changes at the relevant glass transitions. Assuming constant density, the thickness as well as volume fraction of the interfacial layer can be obtained from $\Delta C_{p,\,high}$ and $\Delta C_{p,\,low}$. The results are presented in Table 2.

Table 2 Effect of pore size on T_g, ΔC_p, interaction layer thickness and volume fraction of $T_{g,\,high}$.

Pore size d (nm)	$T_{g,\,low}$[a] (°C)	$T_{g,\,high}$ (°C)	$\Delta C_{p,\,low}$ (J/g K)	$\Delta C_{p,\,high}$ (J/g K)	$\Delta C_{p,\,total}$ (J/g K)	Interaction layer thickness (nm)[b]	volume fraction of $T_{g,\,high}$
7.5	15.4±2.7	NA	NA	NA	0.358±0.005	NA	NA
12	13.6±0.3	49.7±1.4	0.337±0.020	0.034±0.014	0.371±0.005	0.28±0.12	0.07±0.03
16	16.3±0.5	52.9±1.5	0.300±0.019	0.078±0.011	0.378±0.007	0.87±0.12	0.16±0.02
22.6	17.9±0.1	48.4±0.6	0.270±0.013	0.099±0.014	0.369±0.001	1.63±0.24	0.20±0.03
46.6	22.1±0.9	50.7±0.5	0.252±0.004	0.113±0.017	0.365±0.014	3.94±0.49	0.23±0.03
50	23.8±0.1	48.1±0.7	0.262±0.021	0.111±0.012	0.373±0.02	4.05±0.24	0.22±0.01
96.6	27.2±1.0	49.2±2.2	0.282±0.011	0.093±0.008	0.375±0.007	6.42±0.47	0.19±0.01
111	27.9±1.1	48.2±1.2	0.289±0.095	0.097±0.011	0.386±0.010	7.48±0.71	0.19±0.02
198	31.8±0.6	48.4±1.3	0.277±0.004	0.098±0.007	0.375±0.002	13.91±1.00	0.20±0.01
bulk	38.3±0.2	NA	NA	NA	0.370±0.028	NA	NA

a. Mean of data ± standard deviation. Standard deviation is obtained from multiple measurement for two different samples.

b. Thickness $l = d\,\{1-(1-\Delta C_{p,\,high}/\Delta C_{p,\,total})^{1/2}\}/2$, where d = pore diameter

The T_g reduction accompanying the decreasing pore size mentioned above is usually presented in a linear plot of T_g versus 1/d (pore diameter) [23, 26, 73], in analogy to the Gibbs-Thomson analysis, in which melting temperature T_m is linearly depressed with reciprocal of crystal size (see equation 8). However, the relationship between T_g and 1/d does not have a similar strict linear behavior. In the case of NIF, as shown in Figure 4(A), a linear relationship is inadequate to describe T_g versus 1/d. However the relationship can be linearized by plotting $T_{g,low}$ versus log (d), as shown in Figure 4(B). Such a dependence is different from the reported power law for the T_g reduction in polymer ultra-thin films, where the T_g depression with thickness can be expressed as[74, 75]: $T_g = T_g(\infty)\{1 - (\frac{A}{d})^{\delta}\}$, with fitting parameters A and δ. Though, as shown in Figure 4(B) it may be consistent with data reported for freely standing films in which ΔT_g appears linear in the logarithm of film thickness[76]. From Figure 4(B), the equation can be expressed as:$T_g = T_{g,bulk}(A + \delta \log(d))$, where in this case, $\delta = 0.047, \mathrm{A} = 0.87$. On the other hand, the $T_{g,high}$ was only weakly dependent on pore size, as shown in Figure 4(C). Both the behaviors of $T_{g,low}$ and $T_{g,high}$ are consistent with prior work done by Lopez and Simon [72] where it was reported that as the $T_{g,low}$ decreased with decreasing diameter, the dependence of $T_{g,high}$ on pore size remained relatively weak.

From the shell and core model discussed above, the interaction layer with the pore wall accounts for the high T_g. As shown in Figure 4(D). It can be seen that, the thickness of the interaction layer decreases as pore size decreases, which leads to an assumption that, in the smaller pores, the material is more uniform. However, upon examination of the volume fraction of the interaction layer, we see that above 16nm, it is relatively constant. But it seems to decrease rapidly from the pore diameter of 22.6nm where v_f=0.20 to v_f = 0.16 at d =16nm and then to v_f =0.07 for d =12nm. The results for d > 16nm are consistent with the prior work by Lopez and Simon who reported the volume fraction of the surface layer to be independent of pore size [72]. A possible reason for the differences at the small pore size is related to the further observation that as size decreases to 7.5nm, only one T_g is observed in the NIF system, i.e., the surface interaction layer seems to become like the core material.

3.3 Crystallization and Melting

3.3.1 Bulk NIF crystallization

The crystallization of NIF is widely studied and there are literature reports that NIF is able to crystallize below T_g, with the crystal growth rate increasing as T increases towards T_g [41, 45, 46]. In the present work, the main focus is on crystallization inhibition upon heating from the glassy to the supercooled liquid state. When the bulk NIF was cooled from above T_m to 60 ^oC below T_g, no exothermal peak was observed during cooling when the cooling rate ≥ 10K/min, indicating no crystallization during cooling. The reheating curve is shown in Figure 3(A) and for bulk NIF with 10K/min heating rate, an exothermal cold crystallization peak is observed at approximately 100 ^oC. This response was observed for cooling rates from 10K/min to 30K/min, consistent with prior works on bulk crystallization of NIF [42, 45, 46]. This can be interpreted to imply that even though crystallization is avoided during rapid cooling, nucleation is not suppressed. Therefore, cold crystallization can still occur when the NIF is reheated to above T_g. Prior work suggests that, a rapid cooling rate is necessary to fully suppress nucleation, in such a case, cold crystallization would not be expected during re-heating [11, 77, 78].

3.3.2 Nanoconfined NIF crystallization

Similar to the glass transition behavior, crystallization of nanoconfined NIF also shows a strong pore size dependence. When the pore size is above 22.6 nm, a cold crystallization is observed during reheating, followed by a corresponding melting peak. The cold crystallization temperature T_c, melting temperature T_m and heat of fusion ΔH_m for cold-crystallization and melting varied with pore size. When pore size was reduced to 7.5 and 12 nm, neither cold-crystallization nor melting were observed during re-heating. Even when the cooling rate was as low as 1K/min, cold crystallization and melting were not observed in the heating curves. For the 16nm confined NIF, a barely detectable endothermal melting appeared at approximately 150 ^oC, and for a pore size of 22.6nm and above, crystallization and melting are apparent, as shown in Figure 3(A).

The absence of cold-crystallization and melting for NIF confined in the 12 and 7.5 nm pores indicates that, nucleation, which occurs for the bulk sample, is effectively suppressed by the nano-confinement. To further verify this, we investigated the 12 and 50 nm confined NIF by performing isothermal crystallization experiments: in the DSC, the samples were directly cooled (cooling rate= 30K/min) to the annealing temperature T_a at 100 °C (50nm) and 120 °C (12nm and 50nm) for 2 hours, before cooled to -20 °C and then heated (heating rate=10K/min) back to 180 °C. The T_a values of 100°C and 120°C were chosen to be the onset temperature and peak temperature of the cold crystallization peak for the 50nm confined NIF.

Figure 5(A) shows that, subsequent to annealing at 120°C for 2 hours, the 12nm confined NIF exhibits neither crystallization nor melting upon heating, as seen in curves (I); On the other hand, both crystallization and melting are seen for the 50nm confined NIF treated at both 100°C and 120°C as seen in II and III. Another interesting observation is that, for the 50nm confined NIF, the crystallization and melting behaviors differ depending on T_a. As seen in Figure 5(B) curves (II), for the 50nm confined NIF that has been treated at 120 °C , upon re-heating, two melting peaks are visible in the plots; however, for (III), which is the same sample but treated at 100 °C, only one melting peak is observed. The only difference between treatments is the annealing temperature, and thus, one of the melting peaks appearing in curves (III) can be recognized as a response of a new polymorph of NIF, as discussed subsequently.

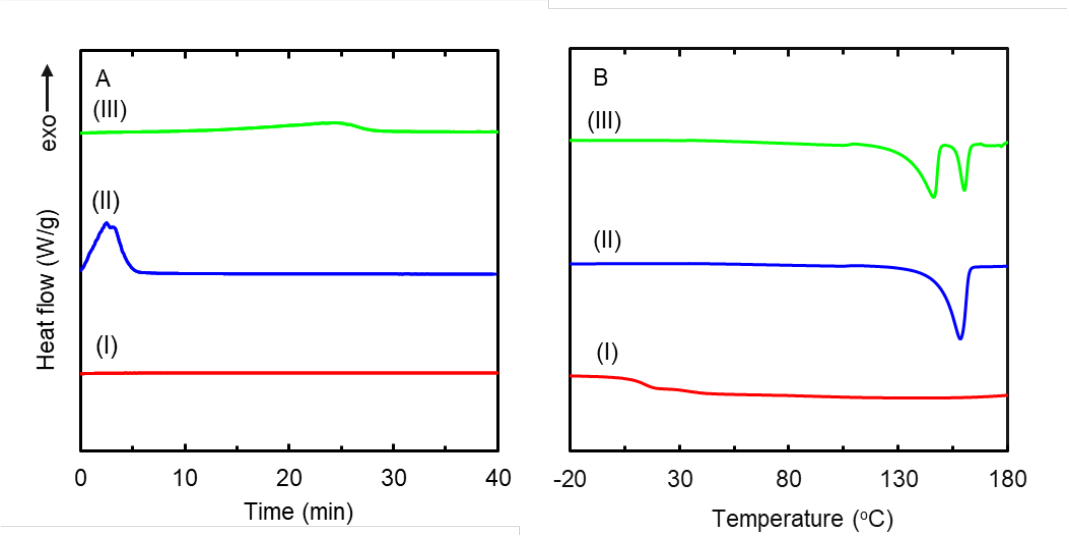

Figure 5. DSC thermograms: A. isothermal curve of crystallization (only 40min is plotted because it better illustrates the crystallization peak); B. heating at 10K/min after isothermal crystallization. (I) NIF in 12nm CPG annealed at 120°C for 120 mins; (II) NIF in 50 nm CPG, annealed at 120°C for 120 mins; (III) NIF in 50nm CPG, annealed at 100°C and for 120 mins

PXRD was also employed to try to further identify the morphology of the 12nm confined NIF, both the amorphous bulk and the 12nm confined NIF were investigated, and the results are shown in Figure 1. After quenching, both bulk and 12nm confined NIF show typical amorphous patterns (Figures 1B and 1D). During the 100°C annealing treatment in a vacuum oven for 2 hours, the bulk NIF starts to crystallize and gives an A-form-like PXRD pattern as shown in Figure1C. However, for the 12nm confined NIF, as seen in Figure 1E, no crystalline pattern is observed, indicating no cold crystallization occurs during the thermal treatment. This result implies that amorphous NIF in the 12nm CPG has higher stability compared to bulk NIF. This result is consistent with the DSC measurement results and will be discussed subsequently. All samples used in the PXRD measurements here were stored at room temperature in a desiccator for 2 days prior to measurement.

These observations demonstrate that the crystallization behavior of NIF in the CPG nano-confinement depends on pore size. In the 12 and 7.5 nm pores, crystallization does not occur during heating, even when cooled slowly or annealed isothermally. Consequently, it suggests that there is an

effective inhibition of crystallization when the NIF is confined below a certain size. The inhibition is unlikely to be due to a lower molecular mobility because the T_g reduction observed in the confined systems is consistent with greater mobility. This behavior is similar to previous findings from Jackson and McKenna[40, 50], where a crystallization suppression in cyclohexane and *o*-terphenyl confined in 4.0 nm and 8.5nm CPGs were reported. In addition, Beiner et.al[39] have reported a similar effect in the pharmaceutical acetaminophen confined in 4.6 nm pores.

A possible explanation here is that the critical nucleus size for the crystallization of NIF is close to the pore diameter[79]. In classical crystallization theory[40], the critical diameter d* for nucleation of a cylindrically shaped nucleus is given by:

$$d^* = (4\sigma_{sl}T_m)/\Delta H_f \rho_s (T_m - T) \quad \textbf{(9)}$$

where T_m is the bulk melting temperature, T is the crystallization temperature, ΔH_f is the heat of fusion, ρ_s is the solid density, σ_{sl} is the solid-liquid interfacial tension (surface energy). Although this equation is usually applied to describe homogeneous nucleation, it can also describe heterogeneous nucleation when no wetting occurs at an interface[40]. In this case, assuming NIF is in the A form, T_m and ΔH_f are obtained from our DSC measurements (for NIF before any thermal treatment), where T_m = 172.3± 0.73 °C, ΔH_f = -104.24 ± 1.70 J/g; σ_{sl} is obtained from applying the Gibbs-Thomson equation, where σ_{sl} = -33.28 ± 2.22 mJ / m^2. The calculation of the critical nucleus diameter d^* for the A form NIF at 100°C is 6.79 ± 0.32 nm, and 8.34 ± 0.55 nm for 120°C. This calculation might be a sufficient explanation for the 7.5nm confined NIF, however, for the 12nm confined NIF, the pore size is larger than the critical nucleus size, hence nucleation suppression may also include other considerations, which is a subject for future study.

3.3.3 Melting Point Depression and Polymorphism

Cold-crystallization and melting peaks appeared during heating (heating rate= 10K/min) for the NIF confined in CPGs with pore size larger than 16 nm. For the 16 nm confinement, only a barely detectable cold-crystallization was observed. The melting was observed on heating and the peak becomes

apparent as confinement size increases. The onset temperature for cold crystallization decreases slightly as pore size decreases and the melting endotherms show a significant melting point depression as pore size decreases as expected from the Gibbs-Thomson equation. For some samples, i.e. pore size greater than 50nm, two endothermal melting peaks appear upon heating. Analysis of the melting temperature with the Gibbs-Thomson size dependence prediction suggests that the melting temperature of the second peak is consistent with the bulk (form A crystal). This is also true of the single melting point samples. Thus, for the samples with two melting peaks, the second peak (high temperature) is recognized as the melting peak of form A, and the first peak is postulated to be a polymorph transition. Detailed information of the onset temperature for cold-crystallization and for melting is given in Table 3.

Table 3. Onset temperature of cold crystallization peaks and melting peaks for different pore size confined NIF. All samples were cooled to -30°C at 10K/min cooling rate before heating with a heating rate of 10K/min.

pore size diameter d (nm)	Cold crystallization temperature (°C)[a]	A form melting point (°C)[b]	Potential new polymorph Melting (°C)
7.5	NA	NA	NA
12	NA	NA	NA
16	104.3 ± 0.4	142.4 ± 0.5	NA
22.6	102.7 ± 1.7	146.7 ± 0.6	NA
46.6	100.6 ± 0.6	153.0 ± 1.3	NA
50	99.4 ± 1.7	157.0 ± 0.2	138.2 ± 0.2
96.6	98.6 ± 0.9	162.3 ± 0.7	145.7 ± 0.2
111	94.4 ± 0.5	162.7 ± 0.8	146.2 ± 0.2
198	92.6 ± 0.2	164.3 ± 0.2	147.1 ± 1.6
bulk	96.4 ± 0.5	166.9 ±0.8	NA

a. The standard deviation determined from three DSC measurements on two different samples.

b. The melting peaks are recognized as A form because they show a reasonable T_m depression tendency as pore diameter decreases

It is interesting to note that, for bulk NIF, the reported T_m of intact A form NIF is 171-173 °C [43, 80-82], however, in this study, after the bulk sample was quenched into the glassy state, the T_m for the

crystal form cold-crystallization is 167ºC, which is slightly lower than the reported value. This phenomenon is similar to what is reported by Miyazaki et.al [44], where they reheated amorphous NIF to above T_m, in their work, the samples share a melting point of around 168ºC, which they related to crystal imperfection.

Figure 6 shows an amplification of the data in the melting regime. For confinement pore sizes of 50, 96.6, 111 and 198nm, two endothermal peaks were observed. Applying the Gibbs-Thomson analysis to the second endotherm (melting point) for all samples, as commented upon above, we find that the T_m values related to the second peak are consistent with the bulk material as depressed in the pores and with those samples exhibiting only a single melting peak. The T_m of the bulk is close to the T_m of crystal form A, thus we interpret it as a melting temperature which is consistent with the bulk (second peak, and samples showing a single T_m) and recognized it to be A form NIF. Fitting of the Gibbs-Thomson Equation to the A form T_m is shown in Figure 7. From the fitting slope, the interfacial tension of the A form is estimated to be σ_{sl}= 33.8 ± 2.2 mJ/m^2. The value is slightly higher than result from molecular dynamic simulations, which give an interfacial tension σ_{sl} = 21.5 ± 1.6 mJ/m^2[83] for NIF.

The extra endothermal peaks for the 50, 96.6, 111 and 198nm confined NIF that emerged before the A form melting peak, on the other hand, are unexpected. To test the possibility of overfilling effects, we overfilled the NIF into the 50nm pore size CPG and did the same measurement. In this case, a third peak appears at the bulk melting point of the NIF. In addition, the emergence of the low temperature melting peak depended on crystallization temperature. Referring to Figure 5: for NIF in the 50nm pores, two endothermal peaks are observed after annealing at 100 ºC, whereas only one melting peak emerges after annealing at 120ºC. These results indicate that, the low temperature endotherm does not result from bulk melting and another explanation is required. We postulate that a stable polymorph accounts for the low temperature endothermal peaks appearing in the NIF confined in pores of size ranging from 50-198 nm. In this case, the low T peaks would be a transformation from a polymorph to A form, with an endodermal heat of transformation.

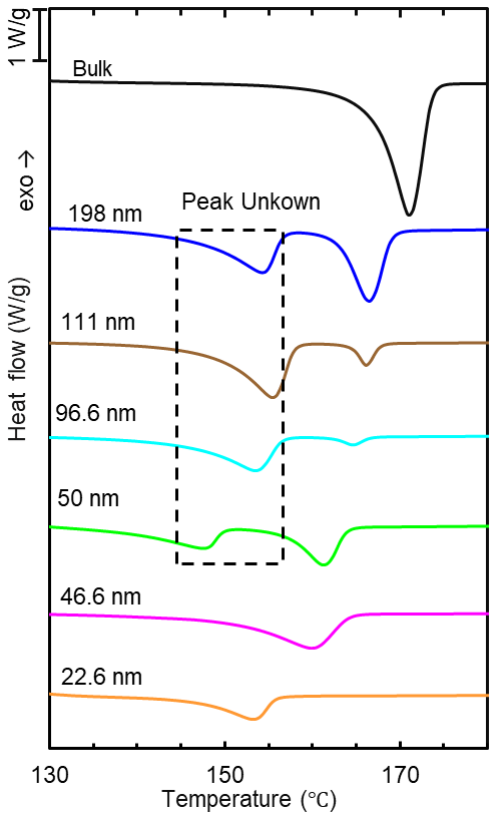

Figure 6. DSC thermograms showing the transformation regions for NIF confined in pore sizes above 22.6nm and for bulk NIF. The first peak is marked as unknown peak, indicating an unknown polymorph transition peak.

It is known that, A form NIF is the most stable crystalline form in the bulk. Other polymorphs of NIF are generally considered as metastable with a tendency to convert to the A form over time. Though, it has been reported that, upon confinement in CPGs or nonporous channel anodic aluminum oxide (AAO), the molecules might have a different nucleation mode, resulting in a more stable polymorph [34, 35, 37, 38, 84]. The formation of different polymorphs is generally considered to be determined by nucleation. Based on classical crystallization theory, after the nuclei achieve a critical size, the nuclei can grow into a crystal[85]. The crystal mature form, i.e. crystal packing and orientation, is an outcome corresponding to the nucleation form[86, 87]. When crystallization occurs under nanoconfinement, the pores have a dimension similar to the critical nucleus size, so it is reasonable to presume that a certain size confinement might regulate the nucleus size, resulting in a selection or stabilization of different

polymorphs[29, 84]. In spite of the fact that the specific mechanism of stabilization and selection of polymorphs in nanoconfinement is still incomplete, studies of their bahaviors provide a potential path to stabilize or even control the formation of polymorphs for specific materials.

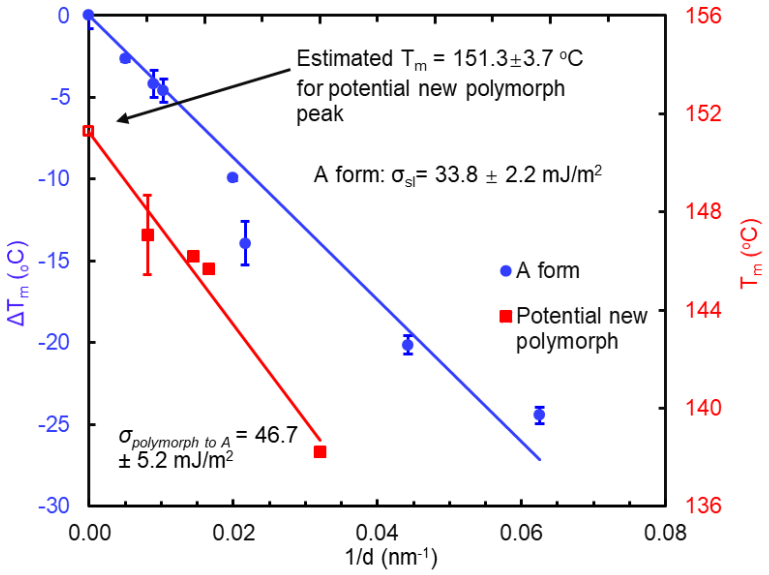

Figure 7. Gibbs-Thompson equation fitting for melting of A form NIF and the unknown low temperature endothermal peak.

In the present work, a low T melting peak emerged in the temperature range 138 to 147 °C, and only one cold-crystallization peak was observed during heating. The total heat of fusion during the cold-crystallization (exotherm) is approximately equal to the sum of heat fusion from the low T peaks and high T peaks (melting of form A). Similar to the A form behavior, the onset temperature of the low T peaks also shows a transformation point depression, which can also be described by the Gibbs Thomson equation, as shown in Figure 7. By assuming that the transition temperature also follows the Gibbs-Thomson relation and applying a linear fitting, the interfacial tension for the crystal-to-crystal interface is estimated as as $\sigma_{polymorph\ to\ A}$ = 46.7 ± 5.2 mJ/m², and the transition temperature in the bulk is estimated by linear extrapolation to be 151.3± 3.7 °C.

According to the literature[61, 80, 88], two metastable polymorphs have been reported for NIF: B (II or β) form with a melting point of around 161-163°C and C (III or γ) form with a melting point reported as 135°C. Neither of these polymorphs has been reported to have a melting or transition point of 151.3± 3.7 °C. Thus, we attribute the low T peak to a transformation of an unknown polymorph to form A in 50- 198nm size nanoconfinement.

4. Summary and Conclusions

The glass transition and crystallization of the pharmaceutical nifedipine confined in nanoporous glass matrixes has been studied by differential scanning calorimetry. NIF confined in nine different pore size CPGs and in the bulk were investigated. The behavior of the glass transition, cold-crystallization and melting were found to depend on the confinement size. For the glass transition, a T_g depression effect was observed in the CPG confined NIF, and the material confined in all but the smallest pore size exhibited two glass transition temperatures consistent with previous studies on porous confined organic molecules. The observations could be described by a two-layer model. For cold-crystallization and melting, when the CPG pore size is smaller than 12nm, cold-crystallization and melting are missing from the 10K/min re-heating thermogram following cooling at the same rate, on the other hand, clear cold-crystallization and melting peaks are observed for the NIF confined to larger pore sizes with the same thermal treatment. The missing of the cold-crystallization peak as well as melting peak is not affected by changing of the thermal conditions, indicating that an effective inhibition of crystallization in NIF when confined at the nanoscale. For NIF under confinement with pore sizes of 50, 96.6, 111 and 198nm, two melting peaks were observed during re-heating. We interpret the low temperature endotherm as providing evidence of a new, previously unreported, isomorph of the confined NIF. Further work is underway to perform structural analysis to establish the crystal structure of the new polymorph observed in nanoconfined NIF.

Acknowledgements The authors are grateful to the National Science Foundation under grant CMMI-1662046 and the John R. Bradford Endowment at Texas Tech University, each for partial support of the work. We also thank Prof. Raj Suryanarayanan for providing us with the nifedipine, Prof. Sindee L.

Simon and Dr. Yung P. Koh for providing help with the DSC measurements and useful discussion on the content of this paper. We also thank Dr. Daniel Unruh help with the on PXRD.

References

1. Wunderlich, B. *Theory of cold crystallization of high polymers.* The Journal of Chemical Physics, 1958. **29**(6): 1395-1404.
2. Dole, M. *Thermodynamic properties of high polymers as a function of their pretreatment as determined by specific heat measurements.* Kolloid-Zeitschrift, 1959. **165**(1): 40-57.
3. Ke, B. *Differential thermal analysis of high polymers. IV. Saturated linear polyesters.* Journal of Applied Polymer Science, 1962. **6**(24): 624-628.
4. Illers, K.H. *Glass transition and cold crystallization in 'even' and 'odd' ω-amino-acid polyamides.* Polymer, 1977. **18**(6): 551-553.
5. Yu, L. *Amorphous pharmaceutical solids: preparation, characterization and stabilization.* Advanced Drug Delivery Reviews, 2001. **48**(1): 27-42.
6. Yoshioka, S. and Aso, Y. *Correlations between Molecular Mobility and Chemical Stability During Storage of Amorphous Pharmaceuticals.* Journal of Pharmaceutical Sciences, 2007. **96**(5): 960-981.
7. Hancock, B.C.; Zografi, G. *Characteristics and significance of the amorphous state in pharmaceutical systems.* Journal of Pharmaceutical Sciences, 1997. **86**(1): 1-12.
8. Sun, Y.; Zhu L.; Wu, T.; Cai, T.; Gunn, E.M.; and Yu, L. *Stability of Amorphous Pharmaceutical Solids: Crystal Growth Mechanisms and Effect of Polymer Additives.* The AAPS Journal, 2012. **14**(3): 380-388.
9. Janssens, S.; Van den Mooter, G. *Review: physical chemistry of solid dispersions.* Journal of Pharmacy and Pharmacology, 2009. **61**(12): 1571-1586.
10. Hancock, B.C.; and Shamblin, S.L. *Molecular mobility of amorphous pharmaceuticals determined using differential scanning calorimetry.* Thermochimica Acta, 2001. **380**(2): 95-107.
11. Baird, J.A.; Van Eerdenbrugh, B.; Taylor, L.S. *A Classification System to Assess the Crystallization Tendency of Organic Molecules from Undercooled Melts.* Journal of Pharmaceutical Sciences, 2010. **99**(9): 3787-3806.
12. Bhattacharya, S. and Suryanarayanan, R. *Local Mobility in Amorphous Pharmaceuticals—Characterization and Implications on Stability.* Journal of Pharmaceutical Sciences, 2009. **98**(9): 2935-2953.
13. Zhou, D.; Zhang, G.G.Z.; Law, D.; Grant, D.J.W.; Schmitt, E.A. *Physical stability of amorphous pharmaceuticals: Importance of configurational thermodynamic quantities and molecular mobility.* Journal of Pharmaceutical Sciences, 2002. **91**(8): 1863-1872.
14. Hancock, B.C.; Shamblin, S.L.; and Zografi, G. *Molecular Mobility of Amorphous Pharmaceutical Solids Below Their Glass Transition Temperatures.* Pharmaceutical Research, 1995. **12**(6): 799-806.
15. Yoshioka, M.; Hancock, B.C.; Zografi, G. *Inhibition of indomethacin crystallization in poly (vinylpyrrolidone) coprecipitates.* Journal of Pharmaceutical Sciences, 1995. **84**(8): 983-986.
16. Matsumoto, T.; Zografi, G. *Physical Properties of Solid Molecular Dispersions of Indomethacin with Poly(vinylpyrrolidone) and Poly(vinylpyrrolidone-co-vinyl-acetate) in Relation to Indomethacin Crystallization.* Pharmaceutical Research, 1999. **16**(11): 1722-1728.
17. Jackson, C.L.; McKenna, G.B. *The glass transition of organic liquids confined to small pores.* Journal of Non-Crystalline Solids, 1991. **131**: 221-224.
18. Schönhals, A.; Goering, H.; Schick, C.; Frick, B.; Zorn, R. *Glass transition of polymers confined to nanoporous glasses.* Colloid and Polymer Science, 2004. **282**(8): 882-891.
19. Koh, Y.P.; Simon, S. L. *Kinetic study of trimerization of monocyanate ester in nanopores.* The Journal of Physical Chemistry B, 2011. **115**(5): 925-932.

20. Koh, Y.P.; Simon, S. L. *Trimerization of monocyanate ester in nanopores.* The Journal of Physical Chemistry B, 2010. **114**(23): 7727-7734.
21. Li, Q.; Simon, S.L. *Curing of bisphenol M dicyanate ester under nanoscale constraint.* Macromolecules, 2008. **41**(4): 1310-1317.
22. Park, J.-Y.; McKenna, G.B. *Size and confinement effects on the glass transition behavior of polystyrene/o-terphenyl polymer solutions.* Physical Review B, 2000. **61**(10): 6667-6676.
23. Li, Q.; Simon, S.L. *Surface chemistry effects on the reactivity and properties of nanoconfined bisphenol M dicyanate ester in controlled pore glass.* Macromolecules, 2009. **42**(10): 3573-3579.
24. Shi, P.; Schach, R.; Munch, E.; Montes, H.; Lequeux, F. *Glass transition distribution in miscible polymer blends: from calorimetry to rheology.* Macromolecules, 2013. **46**(9): 3611-3620.
25. Gao, S.; Koh, Y.P.; Simon, S.L. *Calorimetric glass transition of single polystyrene ultrathin films.* Macromolecules, 2013. **46**(2): 562-570.
26. Zheng, W.; Simon, S.L. *Confinement effects on the glass transition of hydrogen bonded liquids.* The Journal of Chemical Physics, 2007. **127**(19): 194501.
27. Alba-Simionesco, C.; Dosseh, G.; Dumont, E.; Frick, B.; Geil, B.; Morineau, D.; Teboul, V.; Xia, Y. *Confinement of molecular liquids: Consequences on thermodynamic, static and dynamical properties of benzene and toluene.* The European Physical Journal E: Soft Matter and Biological Physics, 2003. **12**(1): 19-28.
28. Diao, Y.; Helgeson, M.E.; Myerson, A.S.; Hatton, T.A.; Doyle, P.S.; Trout, B.L. *Controlled nucleation from solution using polymer microgels.* Journal of the American Chemical Society, 2011. **133**(11): 3756-3759.
29. Jiang, Q.; Ward, M.D. *Crystallization under nanoscale confinement.* Chemical Society Reviews, 2014. **43**(7): 2066-2079.
30. Alcoutlabi, M.; McKenna, G.B. *Effects of confinement on material behaviour at the nanometre size scale.* Journal of Physics: Condensed Matter, 2005. **17**(15): R461.
31. Simon, S. L.; Park, J.-Y.; McKenna, G. B. *Enthalpy recovery of a glass-forming liquid constrained in a nanoporous matrix: Negative pressure effects.* The European Physical Journal E: Soft Matter and Biological Physics, 2002. **8**(2): 209-216.
32. Ellison, C.J.; Torkelson, J.M. *The distribution of glass-transition temperatures in nanoscopically confined glass formers.* Nature Materials, 2003. **2**(10): 695-700.
33. Hamilton, B.D.; Ha, J.-M.; Hillmyer, M.A.; Ward, M.D. *Manipulating crystal growth and polymorphism by confinement in nanoscale crystallization chambers.* Accounts of Chemical Research, 2011. **45**(3): 414-423.
34. Sonnenberger, N.; Anders, N.; Golitsyn, Y.; Steinhart, M.; Enke, D.; Saalwächter, K.; Beiner, M. *Pharmaceutical nanocrystals confined in porous host systems–interfacial effects and amorphous interphases.* Chemical Communications, 2016. **52**(24): 466-4469.
35. Graubner, G.; Rengarajan, G.T; Anders, N.; Sonnenberger, N.; Enke, D.; Beiner, M.; Steinhart, M. *Morphology of porous hosts directs preferred polymorph formation and influences kinetics of solid/solid transitions of confined pharmaceuticals.* Crystal Growth & Design, 2013. **14**(1): 78-86.
36. Ha, J.-M., Hamilton, B.D.; Hillmyer, M.A.; Ward, M.D. *Phase behavior and polymorphism of organic crystals confined within nanoscale chambers.* Crystal Growth & Design, 2009. **9**(11): 4766-4777.
37. Hamilton, B.D.; Hillmyer, M.A.; Ward, M.D. *Glycine polymorphism in nanoscale crystallization chambers.* Crystal Growth & Design, 2008. **8**(9): 3368-3375.
38. Beiner, M.; Rengarajan, G.T.; Pankaj, S.; Enke, D. Steinhart, M.; *Manipulating the crystalline state of pharmaceuticals by nanoconfinement.* Nano letters, 2007. **7**(5): 1381-1385.
39. Rengarajan, G.T.; Enke, D.; Steinhart, M.; Beiner, M. *Stabilization of the amorphous state of pharmaceuticals in nanopores.* Journal of Materials Chemistry, 2008. **18**(22): 2537-2539.
40. Jackson, C.L.; McKenna, G.B.*Vitrification and crystallization of organic liquids confined to nanoscale pores.* Chemistry of Materials, 1996. **8**(8): 2128-2137.

41. Hasebe, M.; Musumeci, D.; Powell, C.T.; Cai, T.; Gunn, E.; Zhu, L.; Yu, L. *Fast surface crystal growth on molecular glasses and its termination by the onset of fluidity.* The Journal of Physical Chemistry B, 2014. **118**(27): 7638-7646.
42. Aso, Y.; Yoshioka, S.; Kojima, S.; *Feasibility of using isothermal microcalorimetry to evaluate the physical stability of amorphous nifedipine and phenobarbital.* Thermochimica Acta, 2001. **380**(2): 199-204.
43. Keymolen, B.; Ford, J.L.; Powell, M.W.; Rajabi-Siahboomi, A.R. *Investigation of the polymorphic transformations from glassy nifedipine.* Thermochimica Acta, 2003. **397**(1): 103-117.
44. Miyazaki, T.; Yoshioka, S.; Aso, Y.; Kawanishi, T. *Crystallization rate of amorphous nifedipine analogues unrelated to the glass transition temperature.* International Journal of Pharmaceutics, 2007. **336**(1): 191-195.
45. Cai, T.; Zhu, L.; Yu, L. *Crystallization of organic glasses: effects of polymer additives on bulk and surface crystal growth in amorphous nifedipine.* Pharmaceutical Research, 2011. **28**(10): 2458-2466.
46. Ishida, H.; Wu, T.; Yu, L. *Sudden rise of crystal growth rate of nifedipine near Tg without and with polyvinylpyrrolidone.* Journal of pharmaceutical sciences, 2007. **96**(5): 1131-1138.
47. Shtukenberg, A.; Freundenthal, J.; Gunn, E.;Yu, L.; Kahr, B. *Glass-crystal growth mode for testosterone propionate.* Crystal Growth & Design, 2011. **11**(10): 4458-4462.
48. Musumeci, D.; Powell, C. T.; Ediger, M. D.;Yu, L. *Termination of solid-state crystal growth in molecular glasses by fluidity.* The Journal of Physical Chemistry Letters, 2014. **5**(10): 1705-1710.
49. Greet, R.J.; Turnbull, D. *Glass transition in o-terphenyl.* The Journal of Chemical Physics, 1967. **46**(4): 1243-1251.
50. Jackson, C.L.; McKenna, G. B. *The melting behavior of organic materials confined in porous solids.* The Journal of Chemical Physics, 1990. **93**(12): 9002-9011.
51. Di, X.; Xu, B.; McKenna, G. B. *The melting behavior of trinitrotoluene nanoconfined in controlled pore glasses.* Journal of Thermal Analysis and Calorimetry, 2013. **113**(2): 533-537.
52. Badrinarayanan, P.; Zheng, W.; Li, Q.; Simon, S. L. *The glass transition temperature versus the fictive temperature.* Journal of Non-Crystalline Solids, 2007. **353**(26): 2603-2612.
53. Moynihan, C.T.; Easteal, A.J.; De Bolt, M.A.; Tucker, J. *Dependence of the fictive temperature of glass on cooling rate.* Journal of the American Ceramic Society, 1976. **59**(1-2): 12 -16.
54. Angell, C.A. *Relaxation in liquids, polymers and plastic crystals—strong/fragile patterns and problems.* Journal of Non-Crystalline Solids, 1991. **131**: 13-31.
55. Gibbs, J.W. *The collected works of J. Willard Gibbs*. 1948, Yale Univ. Press.
56. Thomson, J.J. *Applications of dynamics to physics and chemistry*. 1888: Macmillan.
57. Defay, R., I. Prigogine, A. Bellemans, and D. Everett, *Surface Tension and Adsorption Wiley*. New York, 1966.
58. Xu, B.; Di, X.; McKenna, G. B. *Melting of pentaerythritol tetranitrate (PETN) nanoconfined in controlled pore glasses (CPG).* Journal of Thermal Analysis and Calorimetry, 2013. **113**(2): 539-543.
59. Defay, R.; Prigogine, I. *Tension superficielle et adsorption (Desoer, Liège, 1951); with Bellemans, A., translated by Everett, DH, Surface tension and adsorption*. 1966, Longmans, London.
60. Bortolotti, M.; Lonardelli, I.; Pepponi, G. *Determination of the crystal structure of nifedipine form C by synchrotron powder diffraction.* Acta Crystallographica Section B: Structural Science, 2011. **67**(4): 357-364.
61. Caira, M. R.; Robbertse, Y.; Bergh, J. J.; Song, M.; De Villiers, M.M. *Structural characterization, physicochemical properties, and thermal stability of three crystal forms of nifedipine.* Journal of Pharmaceutical Sciences, 2003. **92**(12): 2519-2533.
62. Klimakow, M.; Rademann, K.; Emmerling, F. *Toward novel pseudo-polymorphs of nifedipine: Elucidation of a slow crystallization process.* Crystal Growth & Design, 2010. **10**(6): 2693-2698.

63. Zhao, H.; Simon, S. L. *Methyl methacrylate polymerization in nanoporous confinement.* Polymer, 2011. **52**(18): 4093-4098.
64. Begum, F.; Zhao, H.; Simon, S. L. *Modeling methyl methacrylate free radical polymerization: Reaction in hydrophilic nanopores.* Polymer, 2012. **53**(15): 3238-3244.
65. Zhao, H.; Simon, S. L. Methyl methacrylate polymerization in nanoporous confinement[J]. Polymer, 2011, **52**(18): 4093-4098.
66. Yukutake, H.; Kobayashi, M.; Otsuka, H.; Takahara, A. *Thermal degradation behavior of polystyrene/magadiite nanocomposites prepared by surface-initiated nitroxide-mediated radical polymerization.* Polymer Journal, 2009. **41**(7): 555-561.
67. Gilman, J.W.; Jackson, C.L.; Morgan, A.B.; Harris, R.; Manias, E.; Giannelis, E.P.; Wuthenow, M.; Hilton, D.; Phillips, S.H. *Flammability properties of polymer− layered-silicate nanocomposites. Polypropylene and polystyrene nanocomposites.* Chemistry of Materials, 2000. **12**(7): 1866-1873.
68. Du, M.; Guo, B.; Jia, D. *Thermal stability and flame retardant effects of halloysite nanotubes on poly (propylene).* European Polymer Journal, 2006. **42**(6): 1362-1369.
69. Gilman, J.W. *Flammability and thermal stability studies of polymer layered-silicate (clay) nanocomposites1.* Applied Clay Science, 1999. **15**(1-2): 31-49.
70. Abudakka, M.; Decker, D. S.; Sutherlin, L. T.; Teeters, D. *Ceramic/polymer interpenetrating networks exhibiting increased ionic conductivity with temperature control of ion conduction for thermal runaway protection.* International Journal of Hydrogen Energy, 2014. **39**(6): 2988-2996.
71. Koh, Y.P.; Li, Q.; Simon, S. L. *Tg and reactivity at the nanoscale.* Thermochimica Acta, 2009. **492**(1-2): 45-50.
72. Lopez, E.; Simon, S. L. *Trimerization Reaction Kinetics and T g Depression of Polycyanurate under Nanoconfinement.* Macromolecules, 2015. **48**(13): 4692-4701.
73. Koh, Y.P.; Li, Q.; Simon, S.L. *Tg and reactivity at the nanoscale.* Thermochimica Acta, 2009. **492**(1): 45-50.
74. Keddie, J.L.; Jones, R.A.; Cory, R.A. *Size-dependent depression of the glass transition temperature in polymer films.* EPL (Europhysics Letters), 1994. **27**(1): 59-64.
75. Keddie, J.; Jones, R.; *Glass Transition Behavior in Ultra-Thin Polystyrene Films.* Israel journal of Chemistry, 1995. **35**(1): 21-26.
76. Shamim, N.; Koh, Y.P.; Simon, S.L.; McKenna, G.B. *Glass transition temperature of thin polycarbonate films measured by flash differential scanning calorimetry.* Journal of Polymer Science Part B: Polymer Physics, 2014. **52**(22): 1462-1468.
77. Marsac, P.J.; Konno, H.; Taylor, L.S. *A Comparison of the Physical Stability of Amorphous Felodipine and Nifedipine Systems.* Pharmaceutical Research, 2006. **23**(10): 2306-2316.
78. Baird, J.A.; Taylor, L.S. *Evaluation of amorphous solid dispersion properties using thermal analysis techniques.* Advanced Drug Delivery Reviews, 2012. **64**(5): 396-421.
79. Ngai, K.L.; Magill, J.H.; Plazek, D.J. *Flow, diffusion and crystallization of supercooled liquids: Revisited.* The Journal of Chemical Physics, 2000. **112**(4): 1887-1892.
80. Grooff, D.; De Villiers, M.M.; Liebenberg, W. *Thermal methods for evaluating polymorphic transitions in nifedipine.* Thermochimica Acta, 2007. **454**(1): 33-42.
81. Gunn, E.; Guzei, I.A.; Cai, T. Yu, L. *Polymorphism of nifedipine: crystal structure and reversible transition of the metastable β polymorph.* Crystal Growth & Design, 2012. **12**(4): 2037-2043.
82. Hirayama, F.; Wang, Z.; Uekama, K.; *Effect of 2-hydroxypropyl-β-cyclodextrin on crystallization and polymorphic transition of nifedipine in solid state.* Pharmaceutical Research, 1994. **11**(12): 1766-1770.
83. Gerges, J.; Affouard, F. *Predictive Calculation of the Crystallization Tendency of Model Pharmaceuticals in the Supercooled State from Molecular Dynamics Simulations.* The Journal of Physical Chemistry B, 2015. **119**(33): 10768-10783.

84. Ha, J.-M.; Hillmyer, M.A.; Ward, M.D. *Thermotropic properties of organic nanocrystals embedded in ultrasmall crystallization chambers.* The Journal of Physical Chemistry B, 2005. **109**(4): 1392-1399.
85. Oxtoby, D.W. *Nucleation of first-order phase transitions.* Accounts of Chemical Research, 1998. **31**(2): 91-97.
86. Rengarajan, G.T.; Enke, D.; Steinhart, M.; Beiner, M. *Size-dependent growth of polymorphs in nanopores and Ostwald's step rule of stages.* Physical Chemistry Chemical Physics, 2011. **13**(48): 21367-21374.
87. Ha, J.-M.; Wolf, J.H.; Hillmyer, M.A.; Ward, M.D. *Polymorph selectivity under nanoscopic confinement.* Journal of the American Chemical Society, 2004. **126**(11): 3382-3383.
88. Aso, Y.; YOSHIOKA, S.; OTSUKA, T.; KOJIMA, S. *The physical stability of amorphous nifedipine determined by isothermal microcalorimetry.* Chemical and Pharmaceutical Bulletin, 1995. **43**(2): 300-303.